Low Temperature Physics/Fizika Nizkikh Temperatur, 2016, v. 42, No. 7, pp. 733–737

Temperature and impurity concentration effects on upconversion luminescence in $LaInO_3$ doped with Er^{3+}

A. Sarakovskis, J. Grube, K. Strals, G. Krieke, M. Springis, N. Mironova-Ulmane, and V. Skvortsova

Institute of Solid State Physics, University of Latvia, LV-1063, Riga, Latvia
E-mail: anatoly@cfi.lu.lv

E.K. Yukhno and L.A. Bashkirov

Belarusian State Technological University, 220006, Minsk, Belarus

Received March 11, 2016, published online May 25, 2016

In this paper a novel method for synthesis of $LaInO_3 : Er^{3+}$ is reported and upconversion luminescence properties of the synthesized material at different temperatures (9–300 K) are studied. The samples were prepared by co-precipitation and subsequent heat treatment of lanthanum, indium and erbium hydroxides. It is shown that the excitation at 980 nm leads to a strong green upconversion luminescence in the material. At the concentrations above 0.1 mol % of Er^{3+} the energy transfer upconversion mechanism of the luminescence becomes evident. Further increase of Er^{3+} content in the material leads to higher red-to-green upconversion luminescence intensity ratio. The mechanisms responsible for the observed variation are discussed.

PACS: 78.47.D– Time resolved spectroscopy;
78.55.–m Photoluminescence, properties and materials;
87.15.mq Luminescence.

Keywords: $LaInO_3$, Er^{3+}, photoluminescence, upconversion luminescence spectra.

1. Introduction

In the last decade, rare-earth doped solid solutions based on $LaInO_3$ have been studied as a material for white light-emitting diodes (LEDs) [1,2]. Luminescence properties of both undoped [3,4] and impurity-doped [5–8] $LaInO_3$ material have been reported still episodically. $LaInO_3$ has also found potential application as solid oxide fuel cell [9–11]. Systematic study of the structure, defect chemistry and oxygen ion migration has been performed by [12].

The semiconducting compound $LaInO_3$ with a bandgap of 3.2 eV belongs to an orthorhombically distorted perovskite-like structure with *Pnma* space group [13]. The structure consists of a three-dimensional sublattice of corner-connected InO_6 octahedra. La^{3+} is in the eightfold coordination of oxygen ions. All the octahedra are sharing their corners and are slightly tilted. As opposed to a cubic perovskite, in $LaInO_3$ there are two crystallographic oxygen ions, two on opposite corners of an octahedron along the *b* axis, and four on the same *ac* plane on this octahedron.

In the last years considerable attention has been devoted to the upconversion luminescence (UCL) [14] in rare-earth doped materials owing to practical applications in visible lasers [15], white light luminophors [16], improvement of the solar cells efficiency [17] and others. Erbium has been much studied in different hosts for luminescence purposes, mainly due to its green ($^4S_{3/2}$–$^4I_{15/2}$), red ($^4F_{9/2}$–$^4I_{15/2}$) and infrared (IR) ($^4I_{13/2}$–$^4I_{15/2}$) emissions [18–21].

In the present work, synthesis of Er^{3+} doped $LaInO_3$ and investigation of UCL has been performed. The temperature impact on the UCL spectra is analyzed, excited state absorption (ESA) and energy transfer upconversion (ETU) mechanisms involved in the upconversion process are studied.

2. Experimental

The $LaInO_3 : Er^{3+}$ samples were prepared using co-precipitation and subsequent heat treatment of hydroxides. The content of Er^{3+} was at 0.01–5 mol %. Stoichiometric

amounts of In_2O_3, La_2O_3 and Er_2O_3 were dissolved in diluted HCl under stirring and heating up to the boiling point of solvent, which resulted in the formation of colorless $InCl_3$, $LaCl_3$ and $ErCl_3$ solutions in water–HCl. Then ammonia liquid was added drop-wise until the precipitate formed.

The precipitate of $La(OH)_3$, $In(OH)_3$ and $Er(OH)_3$ was separated from the solution by vacuum filtration, and the resulting mixture of hydroxides was dried in the air at room temperature (RT) for 24 h. Then the hydroxides were fully ground and heat-treated in an electric furnace at 1250 °C for 1 h to produce the final product of $LaInO_3 : Er^{3+}$.

The UCL was excited by a temperature-controlled laser diode (980 nm, power up to 1 W) and measured by an Andor SR-303i-B spectrometer coupled to iCCD camera Andor iStar. Photoluminescence in the sample was excited by a pulsed solid state laser NT342/3UV (pulse duration ~ 4 ns) from Ekspla (wavelength tunable from 210 nm to 2300 nm, linewidth 4.3 cm^{-1}). The laser wavelength was controlled with accuracy of 0.1 nm. Luminescence spectra were recorded by a CCD camera (Andor DU-401-BV) coupled to Andor SR-303i-B spectrometer. Luminescence decay kinetics was measured by Andor SR-303i-B monochromator coupled to a photomultiplier tube (time resolution better than 20 ns) and digital oscilloscope Tektronix TDS 684A.

The x-ray diffraction (XRD) measurements were carried out on a PANalytical X'Pert Pro diffractometer using Cu K_α tube at the voltage of 40 kV and the current of 30 mA. Sample morphology was examined by Zeiss EVO50 XVP Scanning Electron Microscope (SEM) (15 kV, 100 pA).

3. Results and discussion

The XRD pattern of $LaInO_3 : Er^{3+}$ (2 mol %) is shown in Fig. 1. The peaks could be ascribed exclusively to the $LaInO_3$ crystalline phase. No additional peaks appear in the patterns of the samples at any Er^{3+} concentration, which indicates complete dissolution of Er^{3+} ions in the host material.

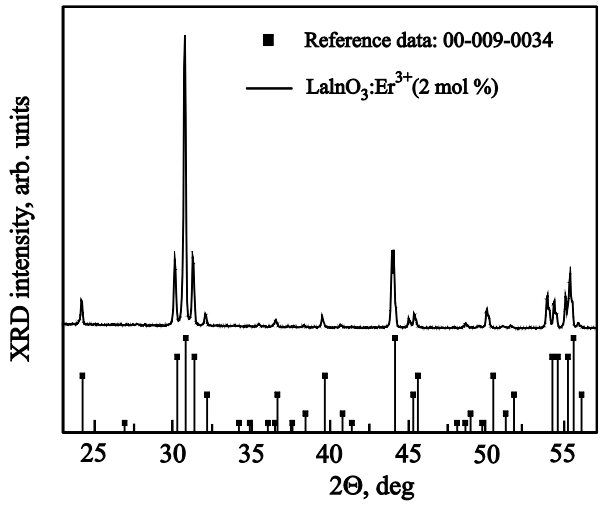

Fig. 1. XRD pattern of $LaInO_3$: Er^{3+} (2 mol %).

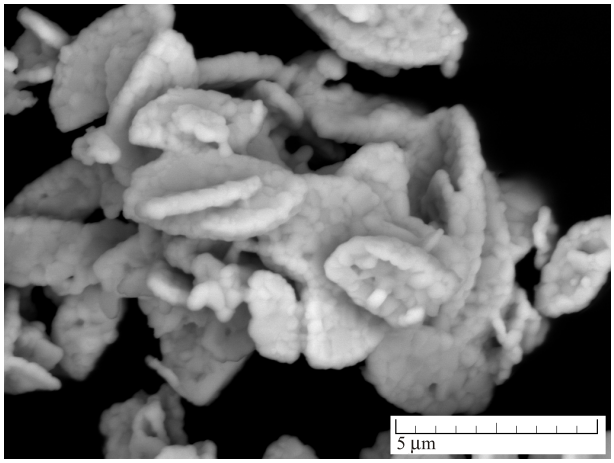

Fig. 2. SEM image of $LaInO_3 : Er^{3+}$ (1 mol %).

The morphology of the samples was studied using SEM (Fig. 2). The synthesized materials have polycrystalline structure and are composed of well-formed crystallites sintered together. The average grain size is in the submicron range.

The photoluminescence spectrum of Er^{3+} doped $LaInO_3$ under excitation at 490 nm (20408 cm^{-1}) is shown in Fig. 3. The sharp lines in the green and red spectral regions can be attributed to $^2H_{11/2} \rightarrow {}^4I_{15/2}$ (530 nm), $^4S_{3/2} \rightarrow {}^4I_{15/2}$ (540 nm) and $^4F_{9/2} \rightarrow {}^4I_{15/2}$ (660 nm) transitions.

Similar luminescence bands have been detected under excitation at 980 nm (10205 cm^{-1}). Figure 4 shows the UCL spectra of $LaInO_3$ with different Er^{3+} ion concentrations. Excitation in the IR region leads to a strong green luminescence at the doping concentrations below 2 mol % while an orange luminescence occurs at the concentrations above 2 mol %.

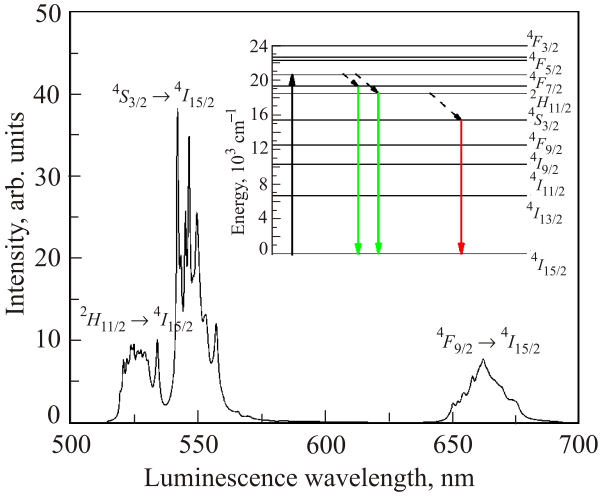

Fig. 3. Luminescence spectrum of $LaInO_3 : Er^{3+}$ (2 mol %) under excitation at 490 nm; measured at RT. Inset shows the energy level diagram and transitions involved in the creation of the luminescence.

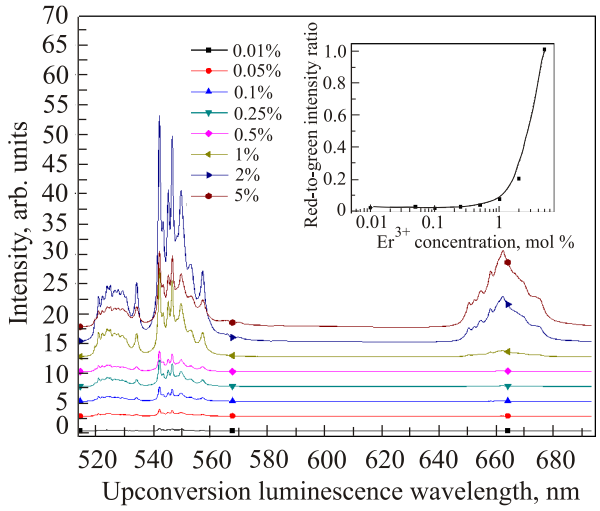

Fig. 4. (Color online) UCL spectra of $LaInO_3$: Er^{3+} under excitation at 980 nm; measured at RT. Inset shows dependence of red-to-green luminescence intensity ratio on the impurity concentration.

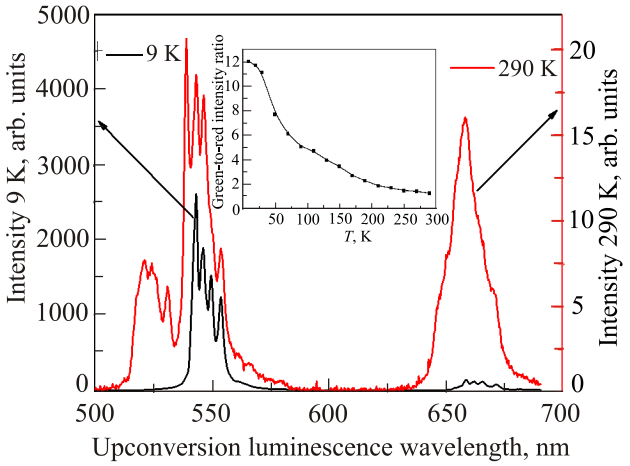

Fig. 6. (Color online) UCL spectrum of $LaInO_3$:Er^{3+} (5 mol %) under excitation at 980 nm (10205 cm^{-1}) measured at different temperatures: 9 K (black) and 290 K (red). Inset: temperature dependence of green-to-red luminescence intensity ratio.

As a rule, in Er^{3+} doped materials either the ESA or the ETU mechanisms are responsible for the appearance of the green UCL band. In ESA, a process of two sequential photon absorption process takes place: $^4I_{15/2} + h\nu \rightarrow {}^4I_{11/2} + h\nu \rightarrow \rightarrow {}^4F_{7/2}$. In ETU process, a successive excitation to $^4I_{11/2}$ level is followed by the nonradiative energy transfer between two erbium ions, which leads to the excitation of one of the ions into $^4F_{7/2}$ and the other undergoes deexcitation to $^4I_{15/2}$ of the other: $(^4I_{11/2}, {}^4I_{11/2}) \rightarrow (^4I_{15/2}, {}^4F_{7/2})$. In the both cases (ESA and ETU) subsequent nonradiative relaxation from $^4F_{7/2}$ to $^2H_{11/2}$ and $^4S_{3/2}$ populates the emitting levels of the green luminescence and the luminescence occurs [22,23]. As observed in the luminescence spectra, the ratio of red-to-green luminescence increases with the rise of impurity concentration. The observed variations of the luminescence intensities corresponding to the green and red upconversion emissions could be explained by the involvement of several cross relaxation (CR) processes, namely, CR1: $(^4F_{7/2}, {}^4I_{11/2}) \rightarrow (^4F_{9/2}, {}^4F_{9/2})$, CR2: $(^4S_{3/2}, {}^4I_{11/2}) \rightarrow \rightarrow (^4I_{9/2}, {}^4F_{9/2})$ and CR3: $(^4S_{3/2}, {}^4I_{15/2}) \rightarrow (^4I_{13/2}, {}^4I_{9/2})$, which either serve as additional channels to populate the $^4F_{9/2}$ level of Er^{3+} or depopulate $^4S_{3/2}$, leading to the increased value of red-to-green intensity ratio (see Fig. 5).

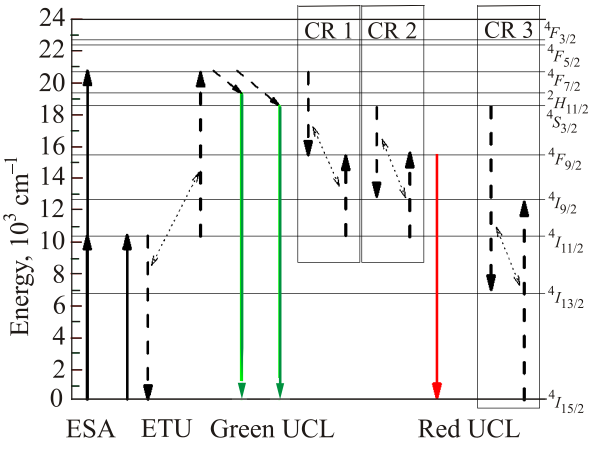

Fig. 5. Energy level diagram of Er^{3+} with possible UCL mechanisms. The absorption and radiative emission processes are indicated by solid lines, nonradiative processes are indicated by dashed and dotted lines.

UCL spectrum measured at low temperature is shown in Fig. 6. As it is seen, the overall intensity of the luminescence measured at low temperature is more than two orders of magnitude higher compared to that measured at RT. This can be explained by a decreased rate of nonradiative transitions in the material. The smaller rate of the nonradiative transitions, particularly, $^4S_{3/2} \rightarrow {}^4F_{9/2}$, is likely to be responsible for higher green-to-red intensity ratio observed when the temperature of the sample is decreased [24].

Additionally, the UCL spectrum measured at low temperature compared to the spectrum at RT lacks the signal at 520 nm. This is due to the fact that at RT the levels responsible for the green luminescence ($^2H_{11/2}$ and $^4S_{3/2}$) are thermally coupled, allowing the level $^2H_{11/2}$ to be thermally populated from $^4S_{3/2}$. At 9 K, the thermal excitation from $^4S_{3/2}$ to $^2H_{11/2}$ level is inefficient and, as the result, the luminescence signal from $^2H_{11/2}$ is vanishingly small [25].

The UCL decay kinetics of the green luminescence (540 nm) excited at 980 nm (10205 cm^{-1}) measured for the samples with different erbium content at RT are shown in Fig. 7.

One can see that the increase of Er^{3+} concentration (above 0.5 mol %) leads to the appearance of an additional slower component in the decay profile of the UCL. Previous studies on Er^{3+} containing materials suggest that the

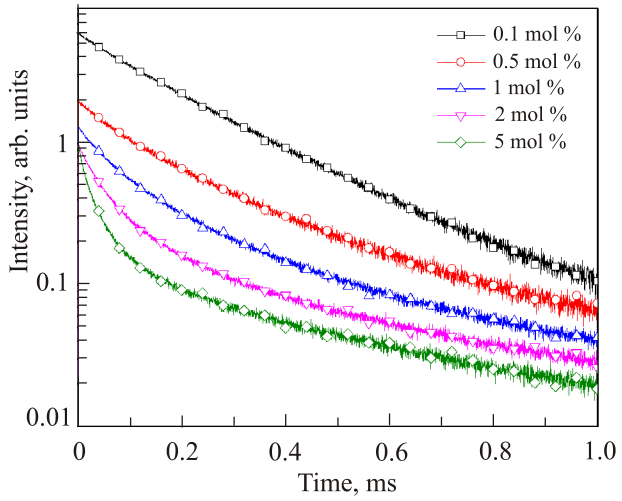

Fig. 7. (Color online) UCL decay kinetics detected at 540 nm under excitation at 980 nm (10205 cm^{-1}) for different Er^{3+} concentrations; measured at RT.

fast component is due to ESA mechanism of UCL, while the slow component is related to ETU processes in the material [25]. One of the decay curves corresponding to Er^{3+} concentration of 2 mol % is shown in Fig. 8.

The initial part of the decay kinetics excited at 980 nm matches well with the decay kinetics measured under direct excitation of $^4F_{7/2}$ level. The characteristic decay time of the fast component ($\tau \sim 100$ μs) is in accordance with the values obtained for $^4S_{3/2}$ level in other Er^{3+} containing systems [22,26]. The decay time of the slower component was estimated to be approximately 1 ms, which is close to the characteristic decay time of $^4I_{11/2}$ reported elsewhere [27], thus confirming the involvement of ETU mechanism in the creation of UCL as indicated in Fig. 5.

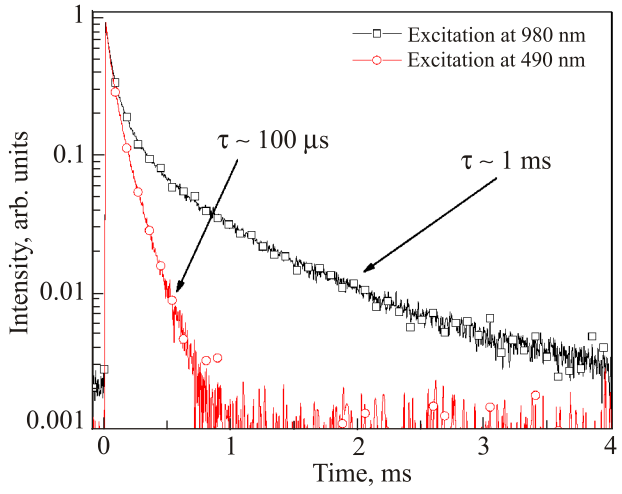

Fig. 8. (Color online) Decay profiles of the luminescence excited at 980 nm (black) and 490 nm (red) for the sample with 2 mol% Er^{3+}; measured at RT.

4. Conclusions

A novel synthesis method of $LaInO_3 : Er^{3+}$ based on co-precipitation and thermal annealing of lanthanum, indium and erbium hydroxides has been developed. The samples emit bright green UCL under IR excitation at 980 nm, which undergoes strong concentration quenching when the concentration of Er^{3+} is above 2 mol %. The dominant UCL mechanism in the samples with low Er^{3+} concentration is ESA; at the concentrations above 0.1 mol % of Er^{3+} the ETU mechanism of the UCL becomes evident. Further increase of Er^{3+} content in $LaInO_3$ leads to enhanced red-to-green UCL intensity ratio, which is explained by the higher rate of cross-relaxation processes in the material. The growth of both UCL intensity and green-to-red ratio of the luminescence observed at lower temperatures is explained by decreased rate of nonradiative transitions in the material.

Acknowledgments

The authors would like to thank the support of Latvian Science Council Grant No. 402/2012 (N.M.-U., V.S.), State research program IMIS2 (M.S.) and the Latvia-Belarus bilateral research project (A.S., L.B.).

1. A. Tang, D. Zhang, L. Yang, and X. Wang, *Optoelectronics and Advanced Materials – Rapid Communications*, **5**, 1031 (2011).
2. X. Liu and J. Lin, *Solid State Sci.* **11**, 2030 (2009).
3. G. Blasse and A. Brill, *Mater. Res. Bull.* **5**, 231 (1970).
4. S.K. Chaluvadi, V. Aswin, P. Kumar, P. Singh, D. Haranath, P.K. Rout, and A. Dogra, *J. Luminescence* **166**, 244 (2015).
5. Xiaoming Liu, Liushui Yan, and Jun Lin, *J. Electrochem. Soc.* **156**, 1 (2009).
6. N. Lakshminarasimhan and U.V. Varadaraju, *Mater. Res. Bull.* **41**, 724 (2006).
7. L.I. Van Steensel, S.G. Bokhove, A.M. Van de Craats, J. De Blank, and G. Blasse, *Mater. Res. Bull.* **30**, 1359 (1995).
8. E.K. Yukhno, L.A. Bashkirov, L.S. Lobanovsky, S.V. Trukhanov, and S.V. Slonskaya, *Inorg. Mater.* **52**, 218 (2016).
9. H. He, X. Huang, and L. Chen, *Solid State Ionics* **130**, 183 (2000).
10. D. Lybye, F.W. Poulsen, and M. Mogensen, *Solid State Ionics* **128**, 91 (2000).
11. K. Nomura and S. Tanase, *Solid State Ionics* **98**, 229 (1997).
12. E. Ruiz-Trejo, E.G. Tavizo'n, and A. Arroyo-Landeros, *J. Phys. Chem. Solids* **64**, 515 (2003).
13. D.B. Rogers, J.M. Honig, and J.B. Goodenough, *Mater. Res. Bull.* **2**, 223 (1967).
14. F. Auzel, *Chem. Rev.* **104**, 139 (2004).
15. F. Tong, W.P. Risk, R.M. Macfarlane, and W. Lenth, *Electron. Lett.* **25**, 1389 (1989).
16. J.E.C. Silva, G.F. de Sa, and P.A. Santa-Cruz, *J. Alloys Comp.* **336**, 323 (2001).

17. A.A. Shalav, B.S. Richards, and M.A. Green, *Solar Energy Materials Solar Cells* **91**, 829 (2007).
18. E. Nogales, B. Mendez, J. Piqueras, R. Plugaru, A. Coraci, and J.A. Garcıa, *J. Phys. D: Appl. Phys*. **35**, 295 (2002).
19. A. Polman, *J. Appl. Phys*. **82**, 1 (1997).
20. H. Przybylinska, W. Jantsch, Y. Suprun-Belevitch, M. Stepikhova, L. Palmetshofer, G. Hendorfer, A. Kozanecki, R.J. Wilson, and B.J. Sealy, *Phys. Rev. B* **54**, 2532 (1996).
21. D. Matsuura, *Appl. Phys. Lett*. **81**, 4526 (2002).
22. A. Sarakovskis, G. Krieke, G. Doke, J. Grube, L. Grinberga, and M. Springis, *Optic. Mater*. **39**, 90 (2015).
23. A. Sarakovskis, J. Grube, A. Mishnev, and M. Springis, *Optic. Mater*. **31**, 1517 (2009).
24. J. Méndez-Ramos, V.K. Tikhomirov, V.D. Rodríguez, and D. Furniss, *J. Alloys Comp*. **440**, 328 (2007).
25. A. Sarakovskis, J. Grube, G. Doke, and M. Springis, *J. Lumin*. **130**, 805 (2010).
26. J.F. Suyver, J. Grimm, M.K. van Veen, D. Biner, K.W. Kramer, and H.U. Gudel, *J. Lumin*. **117**, 1 (2006).
27. J.P. Van Der Ziel, F.W. Ostermayer, and L.G. Van Uitert, *Phys. Rev. B* **2**, 4432 (1970).